KfK 3040 B
Juni 1980

Review of Contributed Papers on Experimentation at LEP

G. Flügge, B. Koppitz, R. Kotthaus, H. Lierl
Institut für Kernphysik

Kernforschungszentrum Karlsruhe

KERNFORSCHUNGSZENTRUM KARLSRUHE

Institut für Kernphysik

KfK 3040 B

Review of Contributed Papers on Experimentation at LEP

G.Flügge[1], B.Koppitz[2], R.Kotthaus[3], H.Lierl[3]

presented by G. Flügge

1) Kernforschungszentrum Karlsruhe, Institut für Kernphysik, und Universität Karlsruhe, Institut für Experimentelle Kernphysik

2) II. Institut für Experimentalphysik, Universität Hamburg

3) Max-Planck-Institut für Physik und Astrophysik München

Invited talk at the International Conference on Experimentation at LEP, Uppsala, Sweden, 16-20 June 1980

Kernforschungszentrum Karlsruhe GmbH, Karlsruhe

Überblick über Beiträge zum Experimentieren bei LEP

Zusammenfassung

Es wird ein Überblick über die Papiere gegeben, die als Beiträge zu dieser Konferenz geschickt wurden. Dabei wird Betonung auf eine vergleichende Beschreibung großer Detektorsysteme und neuerer Entwicklungen von Teilchendetektoren gelegt.

Abstract

Papers contributed to this conference are reviewed. Emphasis is put on a comparative description of large detector systems and recent developments in particle detectors.

1. Introduction

From a total of about 65 abstracts which were submitted to this conference we will review some 40 papers. There are various reasons why several abstracts won't get mentioned. Some papers never arrived or were too late to give us a chance to incorporate them. Others did not at all fit into the context*). Also we had to be somewhat selective to cover the various subjects in 45 min in a comprehensible manner.

Therefore omissions could sometimes not be avoided even for interesting papers. E.g. the subjects of trigger and data acquisition will be totally skipped, also because they were discussed in some detail in the preceding talks this morning.

Since many of the contributions were related to large detectors, either existing or in preparation at storage rings we decided to take the large detectors as a guideline through this talk. In this context, the subjects

i) track detection

ii) calorimetry

iii) hadron identification

will be discussed. New interesting developments aside of the

---

*) An example of this last category is the paper on PEP running experience /1/. The paper gives details about the early experience with PEP, with stored beams up to 11 GeV and luminosities up to 3.4×10^{29} $cm^{-2}s^{-1}$ (by June 1980). To compensate for the short mentioning the paper will be printed in full text in the proceedings.

large detectors will be mentioned along with each of these subjects.

A collection of large detectors which will be looked at is given in table I. Again several detectors are missing in this table, mainly for the following reasons: the first generation of large storage ring detectors like PLUTO and MARK I was not represented in the contributions. The next generation of storage ring detectors at 'low' energies like MARK III /11/, ARGUS /12/, and DM 2 /13/ were considered to be of reduced interest when talking about the very high energy LEP machine. Special devices like the streamer chamber detector UA5 /14/ represent little interest for LEP as well; it has its virtues at high rate hadron interactions for survey type experiments but not at e^+e^- colliders where sophisticated triggering is necessary and interesting events are rare.

As indicated in table I all detectors under consideration (MARK J only for muons) have momentum analysis (chapter 2). It should be mentioned, that nearly half of the solenoids (three out of seven) are equipped (or like CLEO and TPC, will be equipped) with superconducting coils. Difficulties which were reported to this conference, were always due to malfunctioning cryogenic systems /4,15/. The superconducting coils themselves did not present any major problems. Thin superconducting coils ($\lesssim 0.5\ X_0$) at dimensions up to 3.8 m length and 2.3 m diameter prove to be a manageable technique.

All detectors are equipped with electromagnetic calorimeters whereas only few (MARK J and the proton collider experiments) employ

hadron calorimeters (chapter 3).

Muon identification based on range measurement is present in all detectors. We will however not extend on this straightforward technique.

Most detectors have one or several handles on hadron identification as indicated in table I. This is the aspect in which detectors show their strongest differences. A detailed account of hadron identification techniques will be given in chapter 4.

2. Track detection

Most of the large detector systems operating or being installed at colliding beam machines (table I) employ solenoidal magnetic fields parallel to the stored beams for charged particle momentum analysis. Exceptions are the calorimeter MARK J at PETRA and the UA1 detector at the $p\bar{p}$ collider at CERN which will utilize a transverse dipole field of 0.7 T. The majority of detectors (table II) is equipped with copper or aluminium coils producing B-fields of about 0.5 T. The superconducting coils in use allow for fields up to 1.5 T.

The elevated B-field of superconducting magnets facilitates a more compact tracking detector for a given momentum resolution. Moreover novel designs of high current density superconducting coils /4,15/ result in a considerably reduced wall thickness (typically 0.5 X_0 for coil, croystat and insulating material as opposed to more than 1 X_0 for normally conducting coils) and thus interfere

to a much lesser extent with the detection of low energy photons and electrons in electromagnetic calorimeters outside the coil.

Magnetic field volumes are such, that radial track lengths vary between 0.5 m and over 1 m. The solid angle coverage usually exceeds $0.9 \times 4\pi$.

Whereas in the first generation of magnetic detectors at e^+e^--storage rings (MARK I at SPEAR and PLUTO at DORIS and PETRA) cylindrical spark or proportional wire chambers were used, charged particle tracking nowadays primarily relies on cylindrical drift chambers. There are two basic concepts (fig. 1):

Minimal drift chambers:

In these chambers the number of potential wires is kept to a minimum. Drift cells are arranged on cylindrical surfaces. Adjacent sense wires are separated electrostatically by a triplet of potential wires (fig. 2). There are no further field shaping electrodes. The design of minimal drift chambers aims at a simplified construction, high reliability for remote operation and at a low density active volume unobscured by structural material to reduce multiple coulomb scattering as much as possible. Minimal drift chambers were first used in the MARK II detector at SPEAR.

Imaging drift chambers:

record charged particle trajectories by sampling three dimensional space points along the ionization track. The measurement of correlated coordinates is particularly useful to reconstruct events

with high track density like high multiplicity jet events. One example of an imaging drift chamber is the so-called jet-chamber of the JADE detector at PETRA /2/. The cylindrical chamber volume is subdivided into azimuthal sectors by cathode planes. In the median plane of each sector alternating sense and potential wires are strung parallel to the detector and B-field axis. Each sense wire determines a space point (r,ϕ,z) by its position (r), by drift time (ϕ) and charge division (z) measurements. In the JADE detector there are up to 48 samplings per track. The chamber is operated at a pressure of 4 atmospheres primarily to do particle identification by energy loss measurement.

The most radical concept of an imaging drift chamber is the Time Projection Chamber (TPC) developped at Berkeley /7/ (fig. 3). In the TPC the electric drift field is aligned with the magnetic field ($\vec{E} \times \vec{B} = 0$). The E-field forces the ionization electrons to drift onto the chamber endcaps. There, proportional wires and cathode segments ("pads") (fig. 3b) measure the coordinates orthogonal to the drift direction z. The z coordinate is determined by the measured drift time.

The longitudinal B-field greatly reduces the transverse diffusion of the drifting electron swarm thus allowing for a precise position measurement in the plane of magnetic deflection ($r\phi$ plane). For the Berkeley TPC the maximum drift length is 1 m (fig. 3a). Even for such a long drift path a spatial accuracy of about 100 µm in the $r\phi$-plane is expected and was actually achieved in a small test chamber /16/.

There are up to 185 samplings per track in order to determine the particle velocity by dE/dx-measurement. To achieve sufficient dE/dx-accuracy the chamber is operated at a gas pressure of 10 atmospheres.

A simplified version of a TPC (atmospheric pressure, 12 samplings per track, 34 cm maximum drift length) has successfully been taken into operation at TRIUMF to search for the lepton number violating muon decay $\mu^- Z \rightarrow e^- Z$ /17/.

The spatial accuracy obtained by drift time measurement ($r\phi$-determination for all detectors except TPC) is about 200 μm rms in all large systems (table II). This demonstrates that the substantial drift path distortion caused by the uncompensated Lorentz force of the momentum analysing B-field is well understood. As an example fig. 4a shows the space-time relation measured in the MARK II detector for various angles of incidence /6/. For negative (positive) angles the Lorentz force will lengthen (shorten) the drift trajectory relative to the zero field case. This angular dependence does however not significantly affect the spatial resolution as can be seen in fig. 4b. For the CELLO detector it has been shown /18/ that for B-fields as strong as 1.43 T Lorentz force effects are well understood and do not degrade the position measurement.

The spatial accuracy achieved in large detectors is limited by systematic uncertainties like quantization of time digitization, wire displacement due to gravitational and electrostatic forces, alignment errors and others. The inherent spatial resolution of the drift chamber types listed in table II as measured with small prototypes or in single cells is 100 μm or better.

In cylindrical geometry the measurement of the coordinate z along the axis poses a problem. The various techniques used to determine z are:

1) charge division measurement (JADE, AFS): The accuracy of this method is limited by the signal to noise ratio at the preamplifier and is typically $\sigma_z \lesssim 0.01$ x (sense wire length). Though the precision is poor (15-20 mm) the method has the advantage of yielding correlated r, ϕ and z coordinates.
2) Small angle stereo measurement (MARK II, TASSO, CLEO): With sense wires stretched at a small angle of inclination α (3^o-5^o) against the cylinder axis a precision of $\sigma_z = \sigma_{r\phi}/\sin\alpha \simeq$ 3-5 mm is obtained.
3) Cathode readout (CELLO, CLEO): Analog readout of induced charge on angular cathode strips of cylindrical PWC is far superior to charge division and small angle stereo measurement. A resolution of 300 to 400 µm has been achieved in the CELLO /4/ and CLEO /19/ detectors.
4) In the TPC the z coordinate is obtained by drift time measurement.

The momentum precision σ_p/p^2 achieved in the tracking detectors listed in table II varies between 1 and 5% GeV^{-1}. In order to do charge determination for $e^+e^- \to \mu^+\mu^-$ at LEP up to the highest energies a single track accuracy of $\sigma_p/p^2 \lesssim 1\%\ GeV^{-1}$ is necessary.

A promising tool to improve the spatial resolution of large drift chambers by eliminating systematic uncertainties is developping with the observation of ionization by UV Laser light /20/. Primary

ionization of more than 2000 e^-/cm has been observed with a high power N_2-Laser resulting in a narrow pulse height spectrum of 9% FWHM. Ionization tracks could be localized to within 50 μm rms. Though the interpretation of the effect is still somewhat controversial it renders new possibilities for a precise in situ calibration of chambers for accurate space- and dE/dx-measurements in particular inside magnetic fields.

3. Calorimeters

Most papers concerning calorimeters dealt with test and performance of proven techniques in large detectors at e^+e^- and pp colliding rings. (An interesting contribution on the use of streamer tubes in large calorimeters /21/ will appear in full text in the conference proceedings.)

A survey of electromagnetic shower counters presently in use or under construction is given in table III. The relative energy resolutions achieved vary between 8.5% and 16% at 1 GeV impact energy, while the spatial resolutions obtained lie between 2.5 and 10 milliradians. The data show clearly that none of the different calorimeter types used in large facilities is significantly superior to others. In addition two specialized shower counter detectors (Crystal Ball and NA1 Experiment) are included in table III to show what can be achieved with a high degree of specialisation.

The difficulties arising from the use of large cryogenic systems in the technically most ambitious liquid argon solution, have obviously been overcome. This was proven by MARK II at SPEAR and by CELLO and

TASSO at PETRA. CELLO is operating at PETRA with its complete liquid argon system since March 1980. Fig. 5 shows the energy resolution versus the electron energy as measured in a test beam at DESY and with Bhabha scattering at PETRA. γ-ray efficiencies of 60% at 50 MeV and 100% at 110 MeV have been achieved.

One can conclude that the choice for a future experiment will have to be based mutually on physics goals and logistics in the most general sense.

Concerning future developments, several promising attempts have been made. In the sandwich type shower counters, the introduction of imaging techniques is under study. Prototypes of a drift collection calorimeter have been tested by Price /27/ and the principle of TPC has been applied to shower counters by Fischer and Ullaland /28/ in the time-projection quantameter (fig. 6) consisting of a TPC filled with material slabs allowing for shower development. Test results gave a linear response to the electron energy and a resolution of $\sigma/E = 35\%/\sqrt{E}$ was achieved.

Pursuing a prior work /29/, Brisson et al. /30/ have successfully operated a solid argon ionisation chamber at liquid hydrogen temperature ($26^{o}K$). Positive ion effects limit the operation to rates below 1 $mm^{-2}s^{-1}$. Apart from their original aim of inserting such a device into a bubble chamber, their work could be of interest when designing a shower counter very close to a superconductive coil.

The wellknown effect of coherent bremsstrahlung has been used by Del Fabbro and Murtas to build a directional sensitive silicon counter /31/. The detector consists of an 11 cm thick Silicon monocrystal acting as showering material followed by a 2 cm slab of

scintillator to detect the electron cascade. When aligning the 111-direction with the incoming beam, the authors obtain a response more than twice as high as with the crystal rotated by $\gtrsim$ 10 mrad. This is demonstrated in fig. 7 showing the pulse height spectra for different impact energies and crystal orientations. From the measurements one can deduce an angular resolution of $\sim$ 10 mrad, which could for instance be useful for small angle electron tagging.

Experience with large hybrid calorimeters at storage rings and various test measurements have been reported by the MARK J /8/, the AFS /9/, and the UA1 /24/ group. The AFS collaboration has tested a calorimeter prototype consisting of a Uranium scintillator sandwich. The electromagnetic part in front with 5 radiation lengths and the hadronic part of 4 nuclear interaction lengths are read out via different wave length shifter bars. The energy resolution obtained in test beam measurements is $30\%/\sqrt{E}$ and, most important, the response for hadrons and electrons is approximately the same due to the effect of nuclear fission.

In preparation of their hybrid calorimeter (fig. 8) the UA1 collaboration has done extensive tests of prototypes consisting of lead scintillator sandwiches (22.3 X_0) for the electromagnetic and iron scintillator (4.7 absorption lengths) for the hadronic part. Read out is done by use of BBQ bars in both cases. A linear response with beam energy is reported and the energy resolution for hadrons is measured to be $80\%/\sqrt{E}$. Taking into account the response of the electromagnetic part, which increases the total thickness to 5.8 interaction lengths, the resolution improves considerably at low energies.

4. Particle identification

The methods of particle identification currently used are TOF, Cerenkov- and dE/dx measurements. Fig. 9 shows the detector length necessary for various identification methods as a function of the Lorentz factor $\gamma = E/m$. For γ up to 10^3 which is the main region of interest in LEP experiments the C-counter and dE/dx methods are dominant.

There are only two contributions to this conference concerning TOF measurements; one deals with a 2 sr TOF system with no start time signal /32/, the other describes time averaging electronics for large area counters /33/. There was no contribution on transition radiation.

Threshold Cerenkov Counters:

In the last two years there was an attempt to fill the gap in particle identification for γ between 3 and 10 where the TOF method becomes insufficient and atmospheric pressure gas Cerenkov counters do not yet work. This identification gap corresponds to refractive indices n between 1.06 to 1.005.

The development of aerogel which is a sponge-like arrangement of SiO_2 Kernels gave the possibility to produce a light solid medium with quite a small density and with a refractive index between 1.05 and 1.02 /34,35/.

With the adjustment of the aerogel density during the production procedure the refractive index is controlled with an accuracy of about $\pm 2 \cdot 10^{-3}$ /34/ by the amount of solvent, the evaporation pro-

cedure and the heating of the material.

The production process has become reproducible in the past two years with production efficiences of up to 90%. Four big experiments: TASSO /34/, AFS /35/, EHS /36/, and EMC /37/ have initiated the mass production of aerogel blocks of sizes 17 x 17 x 2.3 and 18 x 18 x 3 cm^3 in Hamburg and Lund University respectively.

The yield of photoelectrons was measured /37/ as function of the aerogel thickness d and can be parametrized as $n_{ph.e.} \approx n_{max}(1-e^{-d/\lambda})$ with an absorption length of $\lambda = 12\pm2$ cm.

In large aerogel Cerenkov counters the best light collection was achieved with diffusing walls of MILLIPORE with a reflectivity > 0.9. A yield of up to 6 photoelectrons can be achieved for (β=1) particles depending on the cathode area and the light collection system /34,35,37/. In a smaller system using mirror focussing up to 12 photoelectrons were obtaind /36/.

Figs. 10,11 show two arrangements of threshold Cerenkov counters in big detectors at colliding beam machines /34,35/.

The TASSO Cerenkov counter system covers 20% of 4π. It consists of a 13.5 (18) cm thick aerogel counter (n = 1.022 and 1.025, $n_{ph.e.}$ = 3.8±0.2) in conjunction with two gas Cerenkov counters at atmospheric pressure filled with Freon 114 and CO_2. This combination allows for k/π separation up to 16 GeV/c and p identification up to 30 GeV/c.

The AFS experiment uses 3 C-counters in 1 steradian. There are 4 layers of aerogel (8 cm (5 cm) thick, n = 1.050); a 4.5 atm gas C-counter (n = 1.0045) and a 1 atm gas C-counter (n = 1.0010) both filled with Freon 13.

The operation in high magnetic field and space limitations require a special readout for the aerogel. The light is reflected at semi-cylindrical mirrors behind each aerogel cell and is collected via wavelength shifter bars. The light collection efficiency is 62%.

The total system covers a range of particle identification between 0.5-20 GeV/c.

The successful application of aerogel in full range, large solid angle Cerenkov counter systems is quite encouraging. Limitations which may become more important at LEP energies are the complexity of fine grain large solid angle systems, the marginal photoelectron yield and the material introduced in front of other detectors. It would also be highly desirable to fabricate aerogel with n down to 1.006 to avoid pressurized C-counters for the complete range of proton identification.

Imaging Cerenkov-Counters (CID):

A full account of the present status of the imaging Cerenkov technique was given in the talk of T. Ypsilantis /38/. We only want to add two interesting developments which were reported to this conference. Benot and Meunier /39/ describe a multiplexed spot focussing C-counter where the mechanical diaphragm is replaced by an opto-electronic detector array in the image plane. This results in a largely increased aperture and allows for simultaneous detection of several particles over a broad velocity range.

Another novel type of CID with optical readout /40/ may have its applications for forward detectors in colliding beam experiments.

It uses a lens system to refocus and reduce the mirror image of a CID onto an optical CCD array which is coupled by fiber optics to an image intensifier. It covers a solid angle of 200 x 200 $(mrad)^2$ and works over a γ-range of 20 to 100 for 1 m radiator length.

dE/dx Ionisation Measurement:

Energy loss measurement has become one of the most desirable methods of particle identification in large 4π storage ring detectors. The JADE detector /2/ at PETRA, the AFS experiment /9/ at CERN-ISR and the TPC experiment /16/ at PEP measure the primary ionisation in their central tracking device.

Fig. 12 shows the most probable energy loss for e, μ, π, k, p in 1 cm of Argon at 10 atm as a function of the particle momentum p. There are some papers /42/ concerning dE/dx measurements in the low β-region. We will however concentrate on the region of interest for particle separation of LEP i.e. the relativistic rise of the dE/dx curve.

For a k/p separation in the relativistic rise region a typical resolution of $\sigma \approx 3\%$ is needed. In order to achieve this accuracy Landau fluctuations in the energy loss distribution have to be eliminated. The standard method is multiple dE/dx measurement in normal or pressurized gases and the evaluation of a truncated mean /41/.

The "scaling law": pressure times detector length is an invariant with respect to the dE/dx resolution led to the construction of pressurized, small length dE/dx detectors: JADE /2/, CLEO /43/, and TPC /16/ (table IV).

Fig. 13 shows the dE/dx resolution (FWHM) computed by Allison and Cobb as a function of detector length, sample thickness and number of samples /41/.

The black dots in fig. 13 indicate the performance expected for several large dE/dx detectors (see also table IV).

Recent measurements of Lehraus et al. /44/ seem to indicate a considerable discrepancy between expected and measured dE/dx resolutions. They have measured the dE/dx resolution with 64 samples of 4 cm thickness as function of the gas pressure for different gas mixtures and drift paths up to 41 cm. They observe a clear reduction of the relativistic rise at higher gas pressure and resolutions which are worse than expected by about a factor $\sqrt{2}$.

This corresponds to an equivalent reduction of sampling length by about a factor of 2. The resolution obtained so far in some of the large dE/dx detectors at storage rings is at variance with the expectation by about the same ratio (table IV and fig. 13).

Cluster Counting:

Cluster counting which offers a possible way of ionisation measurement avoiding Landau fluctuations was extensively discussed by A.H. Walenta /45/. We just want to mention two contributions:

A detailed MC study of the primary cluster counting method is presented by Lapique and Piuz /46/. An application of the method to a quark search experiment is presented by Basile et al. /47/. They

demonstrate that cluster counting works in streamer and avalanche chambers: for track lengths of 125 cm they get a r.m.s. resolution of $\sim$ 13%, which can possibly be improved by automatic readout methods.

5. Summary

We can summarize as follows:

Track detection:

- Thin superconducting coils ($\lesssim 0.5\ X_0$) work successfully in large solenoidal detectors.
- Minimal and imaging drift chambers reach a single wire resolution of $\lesssim 100\ \mu$.

  Track resolution however is still of the order of 200 μ only, due to various systematic uncertainties.
- UV laser calibration may help to reduce some of these uncertainties.
- The "ultimate" imaging track device, the TPC, looks promising.

Calorimetry:

- All standard techniques of high energy electromagnetic shower detection (lead glass, lead-scintillator, lead-liquid argon, lead-proportional chambers) have been successfully applied to large detector systems. Energy and space resolution do not show clear superiority of any of the methods over the others.

- The wavelength shifter readout has asserted itself as the best readout technique for scintillator calorimetry in large magnetic detectors.
- Some interesting new developments are:
  - imaging shower counters, which extend the imaging chamber technique to shower detection
  - directional sensitive Silicon counters.

Particle identification:

- Silica aerogel has found large scale application as Cerenkov radiator in medium solid angle spectrometers. Refractive indices in the range of $1.02 \leq n \leq 1.05$ have been mass produced. Yields of about 5 photoelectrons have been achieved in large systems without mirrors, whereas up to 12 photoelectrons have been collected with mirrors in simple geometries.
- dE/dx methods have been implemented in large solid angle detector systems. Resolutions obtained so far are still worse than anticipated. Possible resolution limits inherent to the method (in particular for pressurized systems) are being debated.

References

1. Oddone, P., contribution to this conference
2. JADE Collaboration: Bartel., W. et al., Phys.Lett 88B, 171 (1979)
   Drumm,H. et al., 1980 Wire Chamber Conference, Vienna 1980
   (to be published in Nucl.Instr. and Meth.) and DESY-report 80/38 (1980)
   JADE Collaboration: Bartel., W. et al., contribution to this
   conference
3. TASSO Collaboration: Brandelik, R. et al., Phys.Lett 83B, 261 (1979)
   Boerner, H. et al., DESY-report 80/27 (1980)
4. CELLO Collaboration: Schachter-Radig, M.J., contribution
   to this conference
5. Stone, S., contribution to this conference
6. Davies-White, W. et al., Nucl.Instr. and Meth. 160, 227 (1979)
7. Clark, A.R. et al., SLAC-PUB-5012 (1976)
   Wenzel, W.A., contribution to this conference
8. Barber, D.P. et al., Phys.Rev.Lett. 42, 1110 and 1113 (1978)
   Barber, D.P. et al., contribution to this conference
9. Cockerill, D. et al., contribution to this conference
10. IRubbia, C. (spokesman), CERN (1978) unpublished
11. Hitlin, D., contribution to this conference
12. Hasemann, H. et al., DESY (1978), unpublished
    Schmidt-Parzefall, W. et al., contribution to this conference
13. Augustin, J.E. et al., contribution to this conference
14. Rushbrooke, J.G., contribution to this conference
15. Green, M.A. et al., contribution to this conference
16. Fancher, D. et al., Nucl.Instr. and Meth. 161, 38 (1978)

17. Hargrove, C.K. et al., contribution to this conference
18. de Boer, W. et al., Nucl. Instr. and Meth. 156, 249 (1978)
    de Boer, W. et al., to be published in Nucl. Instr. and Meth.
19. Bridges, D. et al., contribution to this conference
20. Bourotte, J. and Sadoulet, W., CERN-EP/80-14 (1980)
    (submitted to Nucl.Instr. and Meth.)
    Hilke, H.J., CERN/EF/BEAM 80-2 (1980)
    (submitted to Nucl. Instr. and Meth.)
21. Jonker, M. et al., contribution to this conference
22. TASSO Collaboration, contribution to this conference
23. Fabjan, C.W. et al., Nucl.Instr. and Meth. 141, 61 (1979)
24. Corden, M.J. et al., contribution to this conference
25. Bloom, E.D., 1979 Int. Symp. on Lepton and Photon Interactions
    at High Energies, Batavia, 1979
26. Amendolia, S.R. et al., contribution to this conference
27. Price, L.E., contribution to this conference
28. Fischer, H.G. and Ullaland, O., contribution to this conference
29. Cobb, J.H. and Miller, D.J., Nucl. Instr. and Meth. 141, 433 (1977)
30. Brisson, V. et al., contribution to this conference
31. Del Fabbro, R. and Murtas, G.P., contribution to this conference
32. Basile, M. et al., contribution to this conference
33. Theodosiou, E. et al., contribution to this conference
34. Lecompte, P. et al., contribution to this conference
35. Henning, S. et al., contribution to this conference
    Henning, S. and Svensson, L., contribution to this conference
36. Carlsson, P.J. et al., contribution to this conference
37. Arnault, C. et al., contribution to this conference

38. Ypsilantis, P., invited talk at this conference

39. Benot, M. and Meunier, R., contribution to this conference

40. Robinson, B., contribution to this conference

41. Allison, W.W.M. and Cobb, J.H., Oxford University preprint 13/80 (1980)

42. Bamberger, A. et al., contribution to this conference

    Basile, M. et al., contribution to this conference

43. Ehrlich, R. et al., contribution to this conference

44. Lehraus, I. et al., contribution to this conference

45. Walenta, A.H. et al., contribution to this conference, and

    IEEE Trans.Nucl.Sci. NS26, 73 (1979)

46. Lapique, F., Piuz, F., contribution to this conference

47. Basile, M. et al., contribution to this conference

48. Fabian, C.W. and Fischer, H.G., CERN-EP/80-27 (1980)

    (submitted to Reports on Progress in Physics)

Table I: Large Detectors at Colliding Beam Machines

Status		Location	Moment. analys.	e/m Calorim.	Hadron Calorim.	μ Ident.	Hadron Separat.	Reference
operating	JADE	PETRA	+	+		+	TOF, dE/dx	2
operating	TASSO	PETRA	+	+		+	TOF, C	3
operating	CELLO	PETRA	+ sc	+		+	dE/dx	4
operating	CLEO	CESR	+ (sc)	+		+	TOF, C, dE/dx	5
operating	MARK II	SPEAR/PEP	+	+		+	TOF	6
in preparation	TPC	PEP	+ sc	+		+	dE/dx	7
operating	MARK J	PETRA	only myons	+	+	+	-	8
operating	AFS	ISR	+	+	+	+	C, dE/dx	9
in preparation	UA1	$p\bar{p}$ Coll.	+	+	+	+	dE/dx	10

Tabel II: Magnetic Tracking Detectors at Colliding Beam Machines

Type	Magnet	$\frac{\Delta\Omega}{4\pi}$		Track radial length (mm)	Track samplings	Spatial Resol. $r\phi(\sigma)$	Spatial Resol. $z(\sigma)$	σ_p/p^2 %·GeV^{-1}	Reference
imaging DC 4 atm	0.45T	.97	JADE	600	48	180 μ	16mm	3.3	2
minimal DC small $\frac{1}{2}$ stereo	0.5 T	.91	TASSO	855	15	$\geq$ 220 μ	3-4mm	2.2	3
PWC cath.r.o. + min. DC	1.3 T sc	.91	CELLO	530	12 rφ 5 z 5 30°	180 μ	0.4mm	1.5*	4,18
min. DC small $\frac{1}{2}$ stereo	0.5 T (1.5 T sc)+	.96	CLEO	800	17	250 μ	5mm (0.3mm)++	5.0	5
min. DC small $\frac{1}{2}$ stereo	0.4 T	.83	MARK II	1034	16	200 μ	4mm	1.9	6
imag. DC 1 atm	0.5 T	.92	AFS	600	42	250 μ	17mm	2.5	9
imag. DC 10 atm	1.5 T sc	.95	TPC	800	185 dE/dx 15 rφ	100 μ**	≤0.2mm**	∿1.0*	7
imag.	0.7 T Dip.	∿1.	UA1	1120	$\frac{1}{2}$ depend.	drift: 250 μ ch.div.: 8-25mm			10

* Inferred from space resol.

** Small test chamber

\+ in preparation

\++ beam pipe PWC's

Table III: Electromagnetic Calorimeters in Large Colliding Beam Detectors.
The specialised detectors (Crystal Ball and NA1) are added for comparison.

	Type	$\frac{\Delta\Omega}{4\pi}$	Thickness X_0	Energy Res. σ_E/E (%·GeV^{-1})	Angular Res. r.m.s.	Comment	Reference
JADE	Pb gla-	.90	12.5	$\sqrt{(6/\sqrt{E})^2 + 3.5^2}$	7 mrad		2
TASSO	Pb/LAR	.90	14	$10/\sqrt{E}$	2.5 mrad	prototype test	22
CELLO	Pb/LAR	.96	21	$8.5/\sqrt{E}$	4 mrad	prototype test	4
MARK J	Pb/Sc.	$6X_0$:.96 $8X_0$:.85	18	$12/\sqrt{E}$	θ: 3^0-5^0 ϕ: 7^0		8
CLEO	Pb/Prop.T.	.68	10-12				5
MARK II	PB/LAR	.69	14	$11.5/\sqrt{E}$	high E e: 3.6 mrad low E γ: 8 mrad		7
TPC	Pb/MWPC	.98	14	$12/\sqrt{E}$	< 10 mrad*	*granularity	16
AFS	U/Sc.	.71	6				9,23
UA1	Pb/Sc.	~1.	23	$9/\sqrt{E}$			10,24
MARK III	Pb/MWPC	.97	12	$16/\sqrt{E}$			11
Xstal ball	NaJ	.94	16	$2.3/\sqrt[4]{E}$ $(1.2/\sqrt[4]{E})$ **	1^0	**test	25
NA1	Pb glass		20	$\sqrt{(6/\sqrt{E})^2 + 0.5^2}$	2 mm		26

Table IV: dE/dx resolution in large storage ring detectors.

	detector	AFS	JADE	CLEO	TPC
	## samples	42	48	117	185
	pressure (atm)	1	4	3	10
resolution*	expected	∿18%	10%	9%	5.5%
	measured	∿27%	∿15%	∿12%	∿6.5% **

* for pions with full sampling

** estimated from electrons with full sampling

Figure Captions

Fig. 1: Evolution of cylindrical tracking detectors:

(a) cylindrical spark and proportional chambers of first generation magnetic detectors at e^+e^- storage rings

(b) minimal drift chambers

(c) imaging drift chambers with $\vec{E} \cdot \vec{B} = 0$ ("Jet chambers")

(d) imaging drift chambers with $\vec{E} \times \vec{B} = 0$ (Time Projection Chamber TPC).

Fig. 2: Drift cell geometry (a) and electric field distribution inside a drift cell (b) of the minimal drift chambers of the CELLO detector at PETRA.

Fig. 3: The Time Projection Chamber of the PEP4-Experiment

(a) schematic view

(b) schematic view of read out plane consisting of PWC sectors equipped with anode wires and cathode segments ("pads").

Fig. 4: Space-time relationship (a) and rms spatial resolution as a function of angle of incidence (b) as measured in the MARK II detector at PEP (DCA: distance of closest approach).

Fig. 5: Energy resolution of the CELLO Pb/LAR-calorimeter as measured in an e^- beam at DESY with 1 X_0 of passive material in front. The point at 18 GeV has been measured with Bhabha scattering at PETRA /4/.

Fig. 6: Time projection quantameter of Fischer and Ullaland /28/.

Fig. 7: Pulse height distributions measured with a directional sensitive silicon crystal /31/
(a) e^- beam aligned with crystal axis
(b) e^- beam not aligned with crystal axis.

Fig. 8: UA1-hybrid calorimeter prototype /10/.
The electromagnetic calorimeter is a Pb/Scintillator sandwich of 22.3 X_0. The hadron calorimeter is a Fe/Scintillator sandwich of 4.7 absorption lengths. Both calorimeters are read out by wave length shifter bars.

Fig. 9: Detector lengths, required by various particle identification methods as a function of the Lorentz factor $\gamma=E/m$ (taken from C.W. Fabjan and H.G. Fischer /48/).

Fig. 10: Cerenkov counter system of the TASSO detector at PETRA.
A layer of Silica Aerogel counters is followed by 2 layers of atmospheric pressure threshold counters filled with Freon 114 and CO_2 respectively. Shown are the two collinear systems each covering 10% of 4π.

Fig. 11: The AFS detector at the ISR /9/

(a) schematic view of the detector along the beam line

(b) Silica Aerogel Cerenkov counters arranged in 4 layers. The Cerenkov-light is focussed by cylindrical mirrors onto wave length shifter bars.

Fig. 12: Most probable energy loss of e,μ,π,k,p in 1 cm of Argon at 10 atm versus particle momentum. Maximum energy loss differences in the region of the relativistic rise are 16% for π's and k's and 10% for k's and p's.

Fig. 13: Ionisation resolution (FWHM) of multisampling detectors as calculated by Allison and Cobb /41/ for $\beta\gamma = 100$. The black dots mark the expected resolution of several large dE/dx detectors. The arrows indicate the deterioration of the dE/dx accuracy if the effective sampling thickness were only half of the actual value.

Large Tracking Detectors

MARK I, PLUTO :

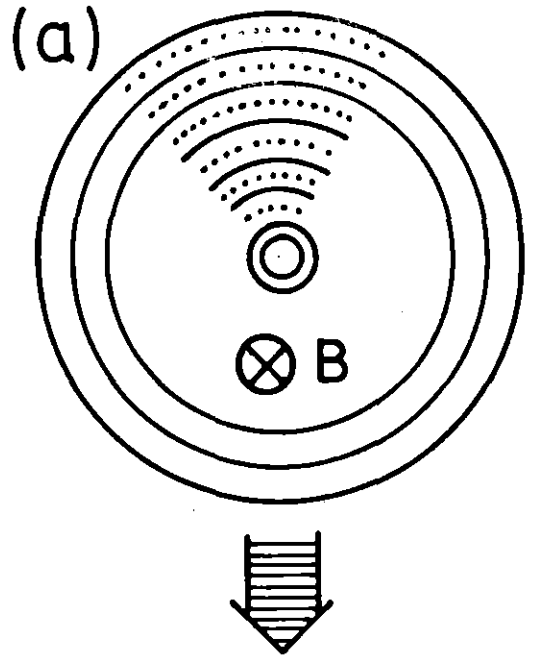

Minimal DC's

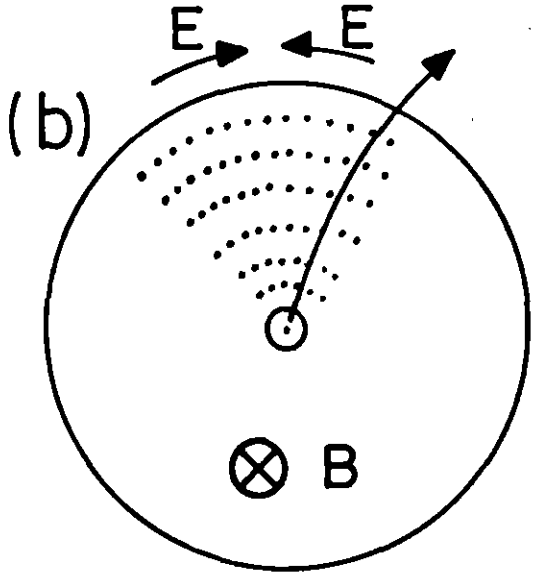

MARK II
TASSO
CELLO
CLEO

Imaging Chambers

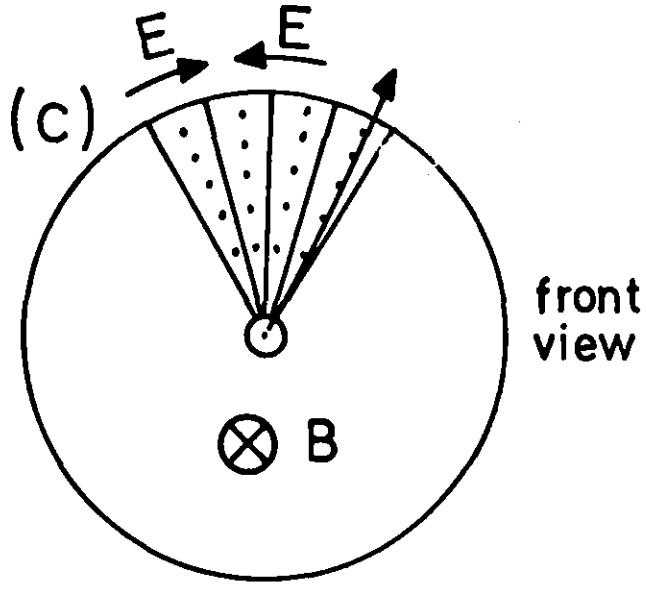

JADE
AFS
MARK III

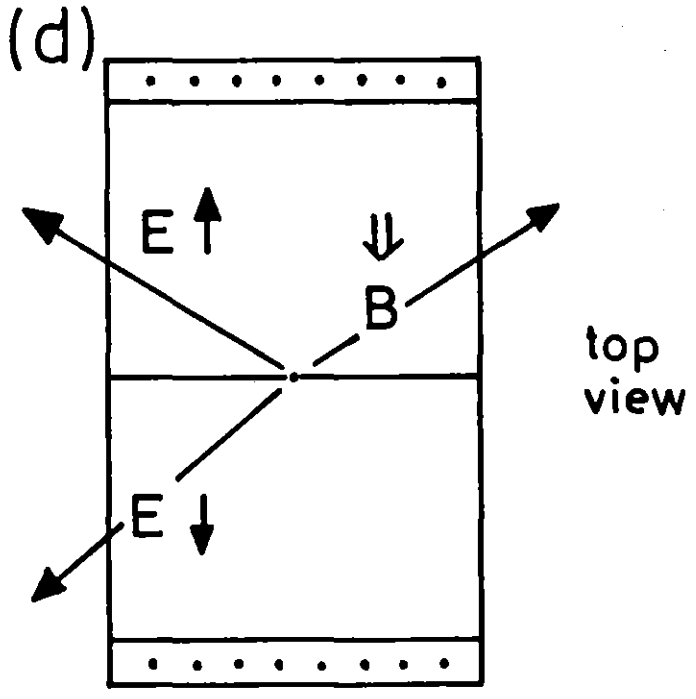

B⇓ TPC: PEP 4
TRIUMF

B ⊗ UA1

Fig. 1

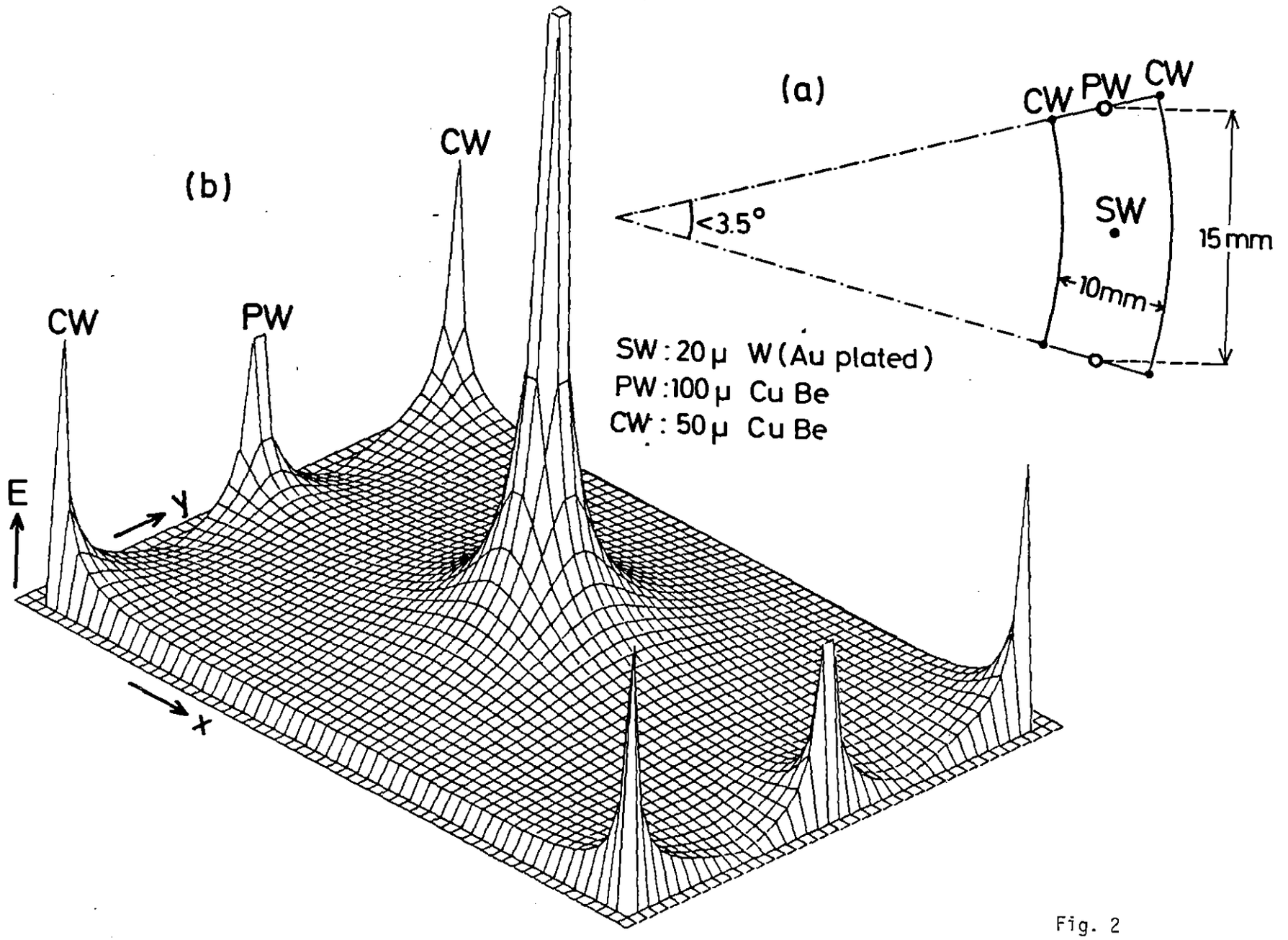
(a)
CW
PW
CW
<3.5°
SW
15mm
10mm
SW : 20 μ W (Au plated)
PW : 100 μ Cu Be
CW : 50 μ Cu Be
(b)
CW
PW
CW
E
y
x

Fig. 2

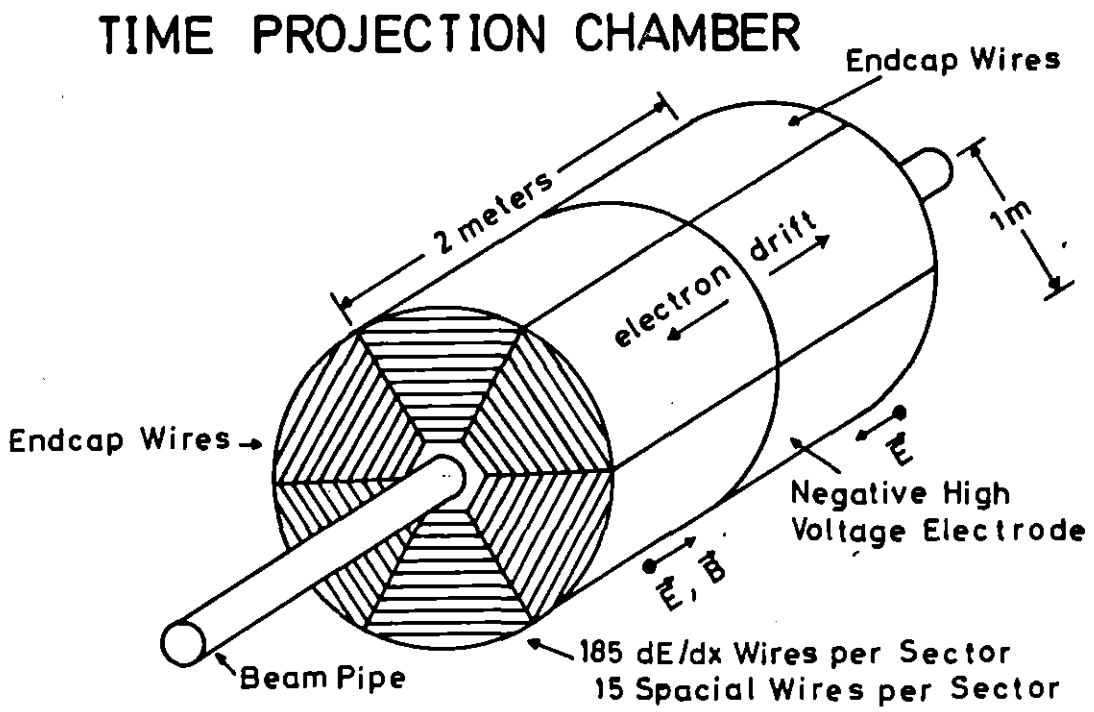
TIME PROJECTION CHAMBER
Endcap Wires
2 meters
1m
drift
electron
Endcap Wires
E
Negative High
Voltage Electrode
E, B
185 dE/dx Wires per Sector
15 Spacial Wires per Sector
Beam Pipe

(a)

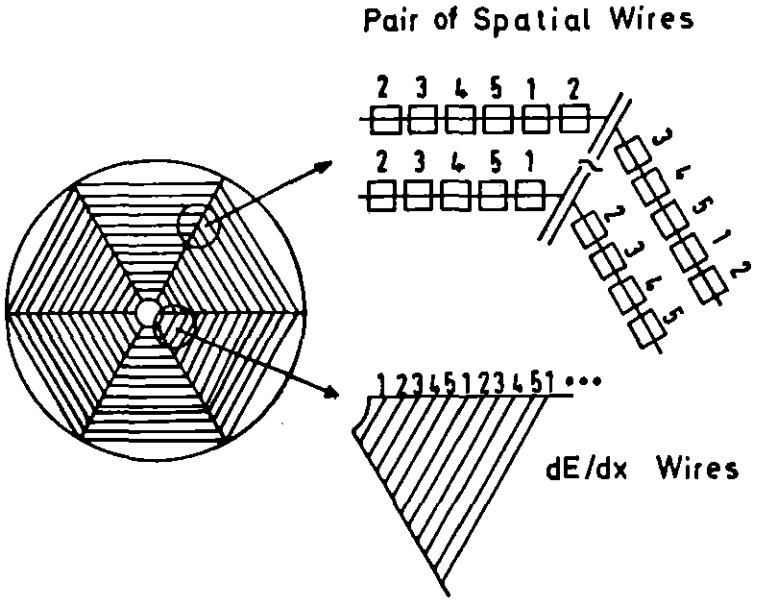
Pair of Spatial Wires
2 3 4 5 1 2
2 3 4 5 1
1 2 3 4 5 1 2 3 4 5 1 ...
dE/dx Wires

(b)

Fig. 3

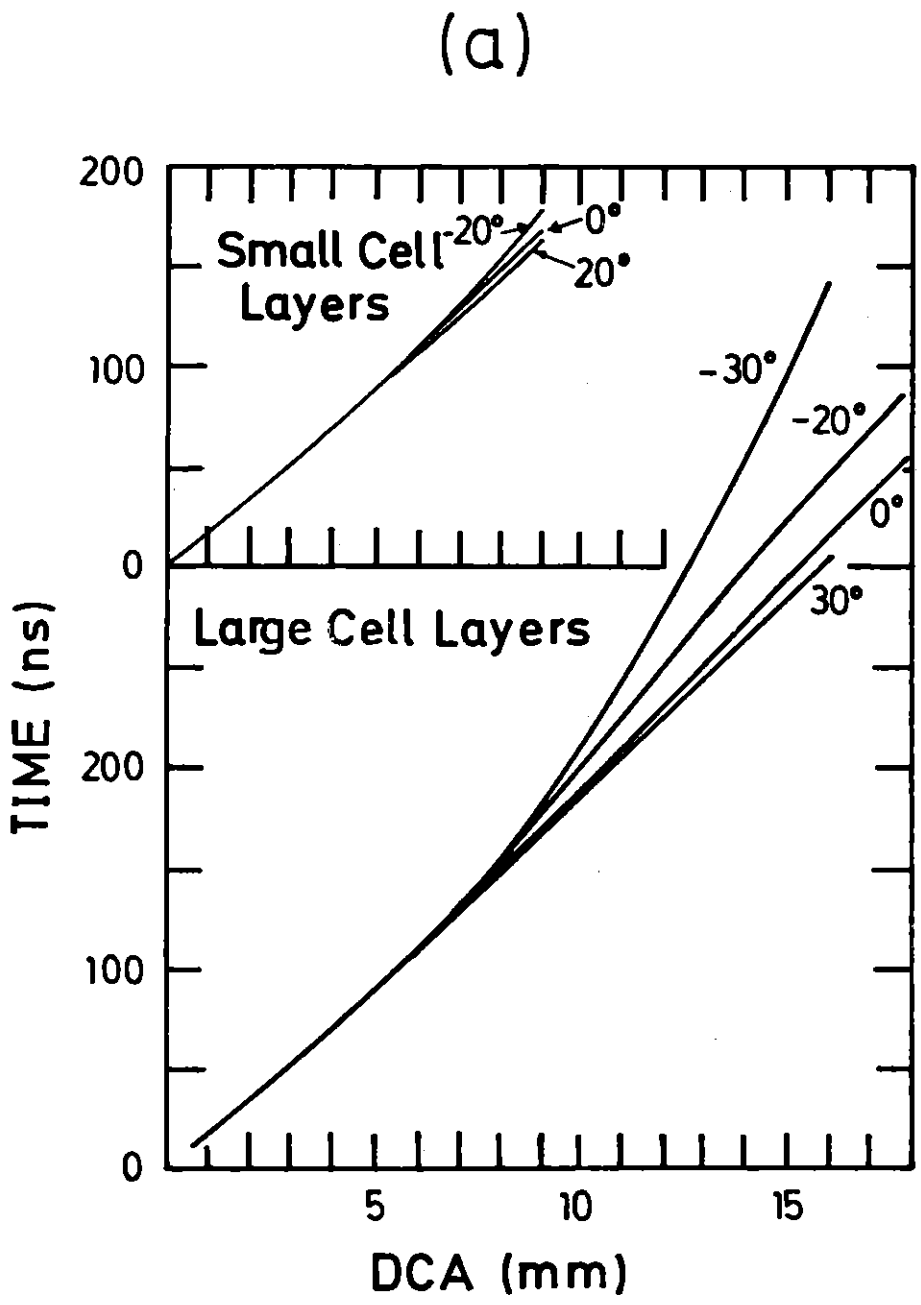
(a)
200
100
0
200
100
0
TIME (ns)
Small Cell Layers
Large Cell Layers
-20°
0°
20°
-30°
-20°
0°
30°
5
10
15
DCA (mm)

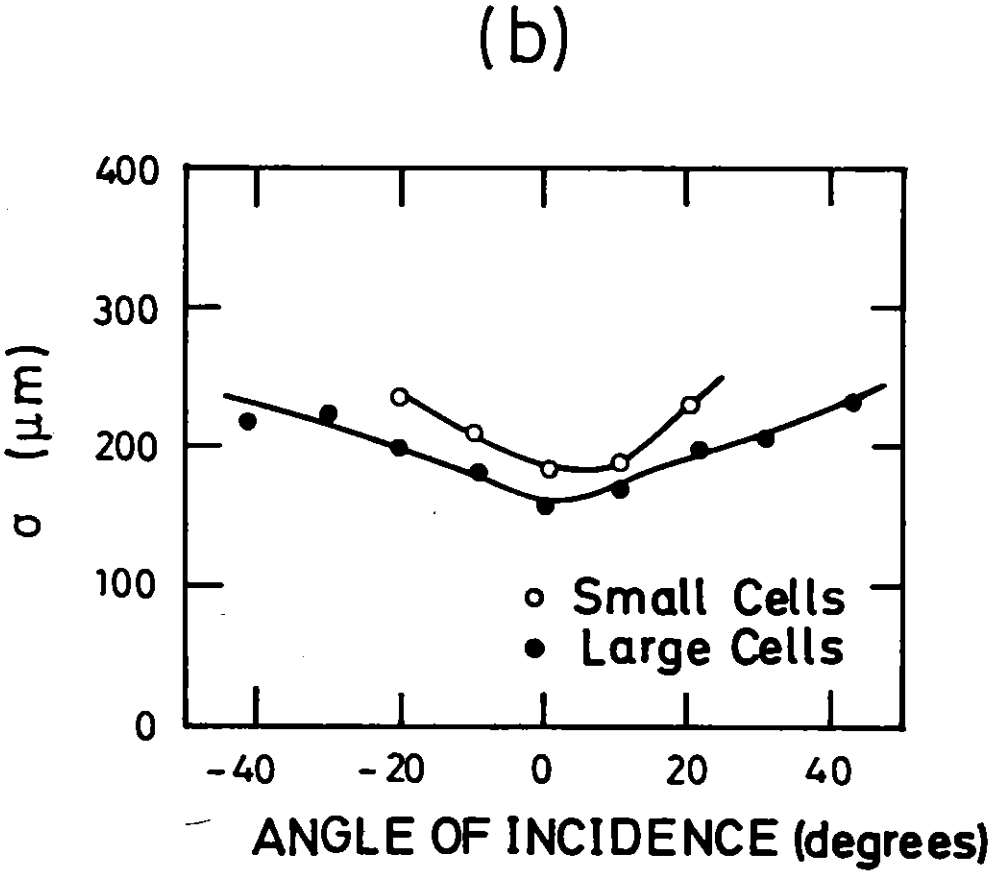
(b)
400
300
200
100
0
σ (μm)
Small Cells
Large Cells
-40
-20
0
20
40
ANGLE OF INCIDENCE (degrees)

Fig. 4

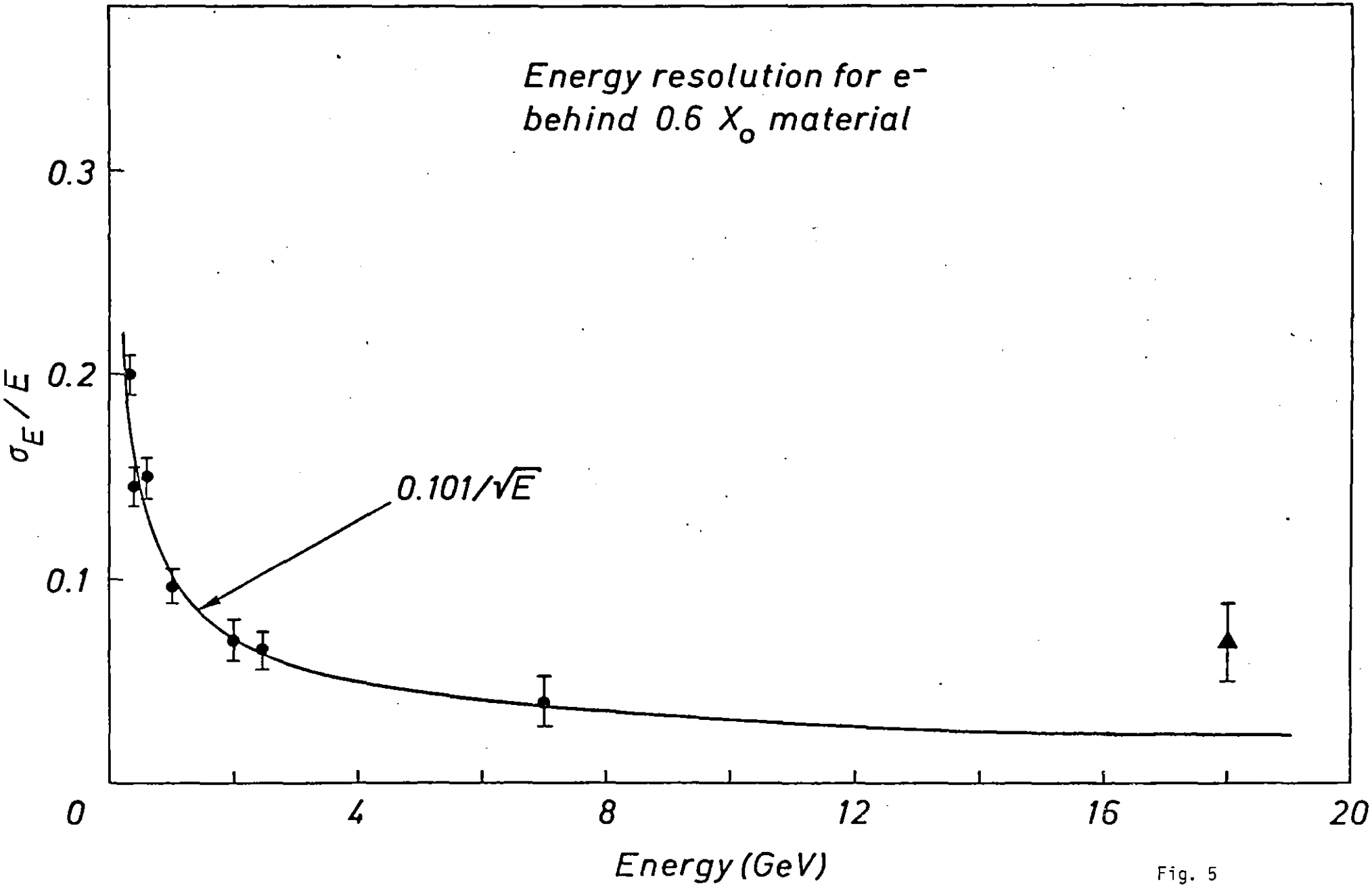
Energy resolution for e⁻
behind 0.6 X₀ material
0.3
0.2
0.1
σE / E
0.101/√E
0
4
8
12
16
20
Energy (GeV)

Fig. 5

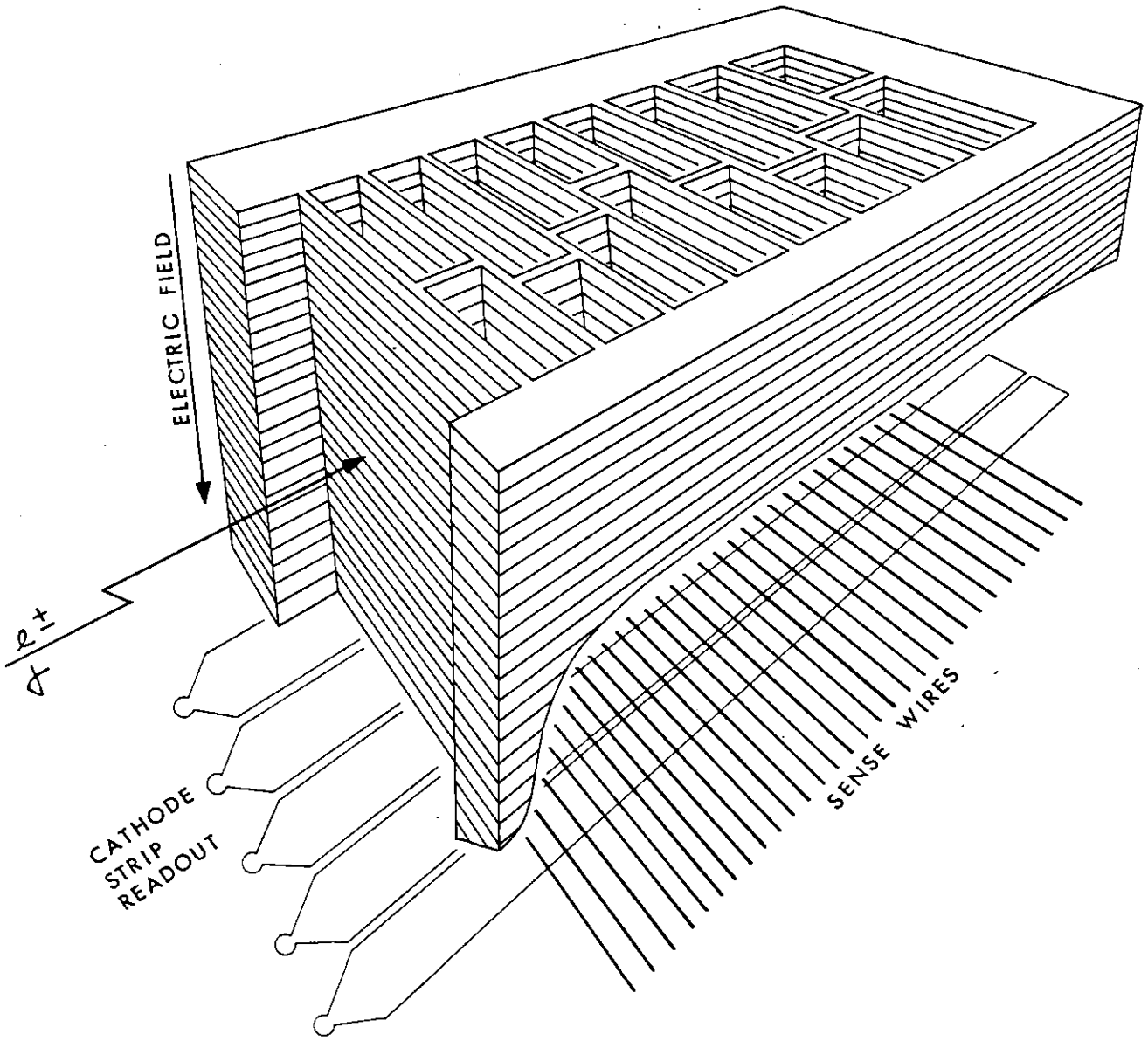
ELECTRIC FIELD
e+
CATHODE
STRIP
READOUT
SENSE WIRES

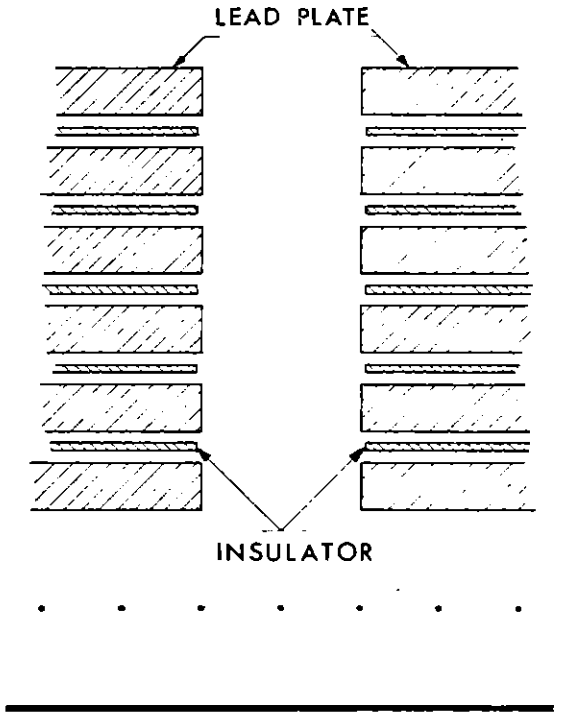
LEAD PLATE
INSULATOR

Fig. 6

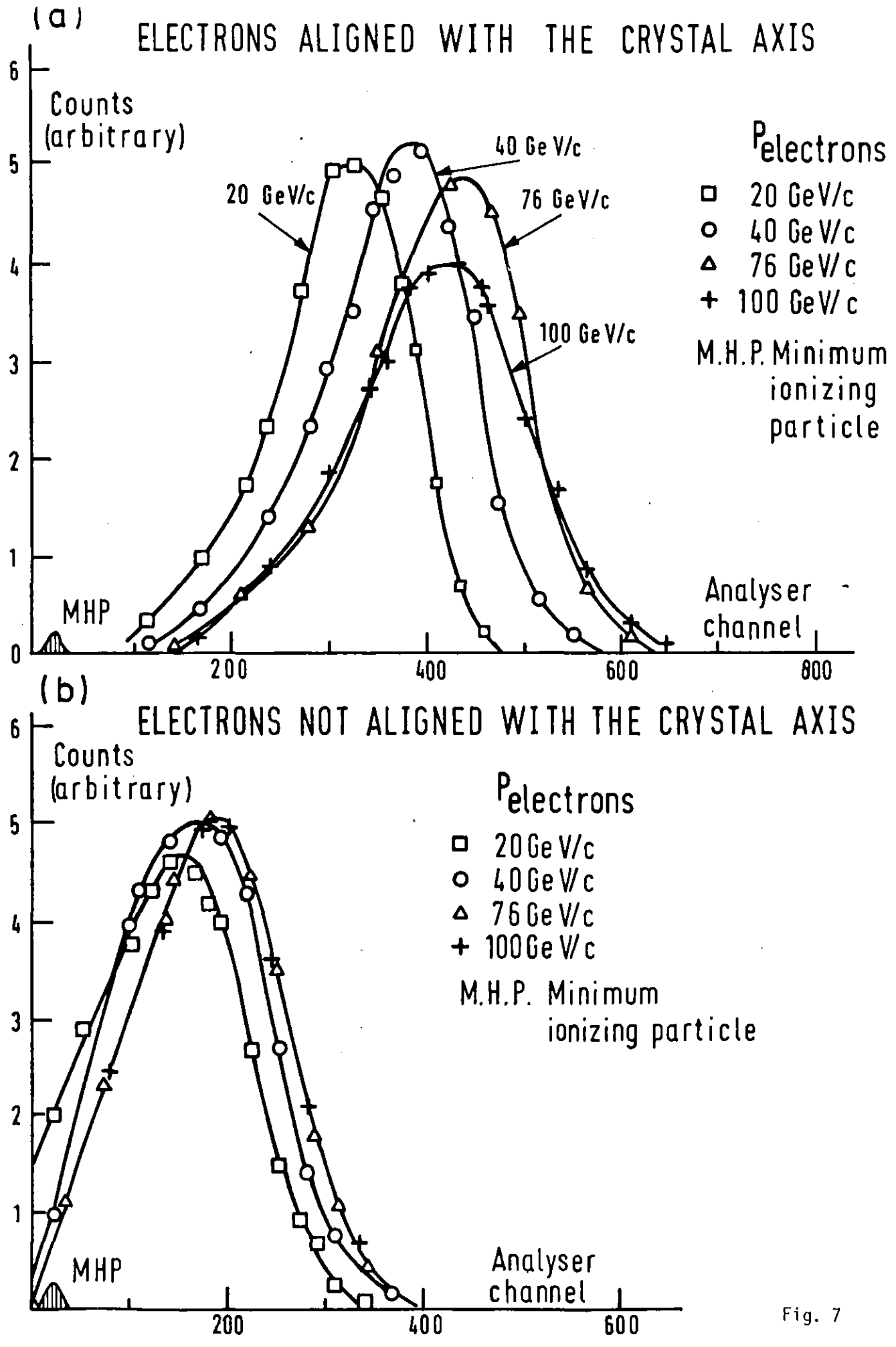
(a)
ELECTRONS ALIGNED WITH THE CRYSTAL AXIS
Counts
(arbitrary)
20 GeV/c
40 GeV/c
76 GeV/c
100 GeV/c
Pelectrons
20 GeV/c
40 GeV/c
76 GeV/c
100 GeV/c
M.H.P. Minimum
ionizing
particle
MHP
Analyser
channel
0
1
2
3
4
5
6
200
400
600
800
(b)
ELECTRONS NOT ALIGNED WITH THE CRYSTAL AXIS
Counts
(arbitrary)
Pelectrons
20 GeV/c
40 GeV/c
76 GeV/c
100 GeV/c
M.H.P. Minimum
ionizing particle
MHP
Analyser
channel
1
2
3
4
5
6
200
400
600

Fig. 7

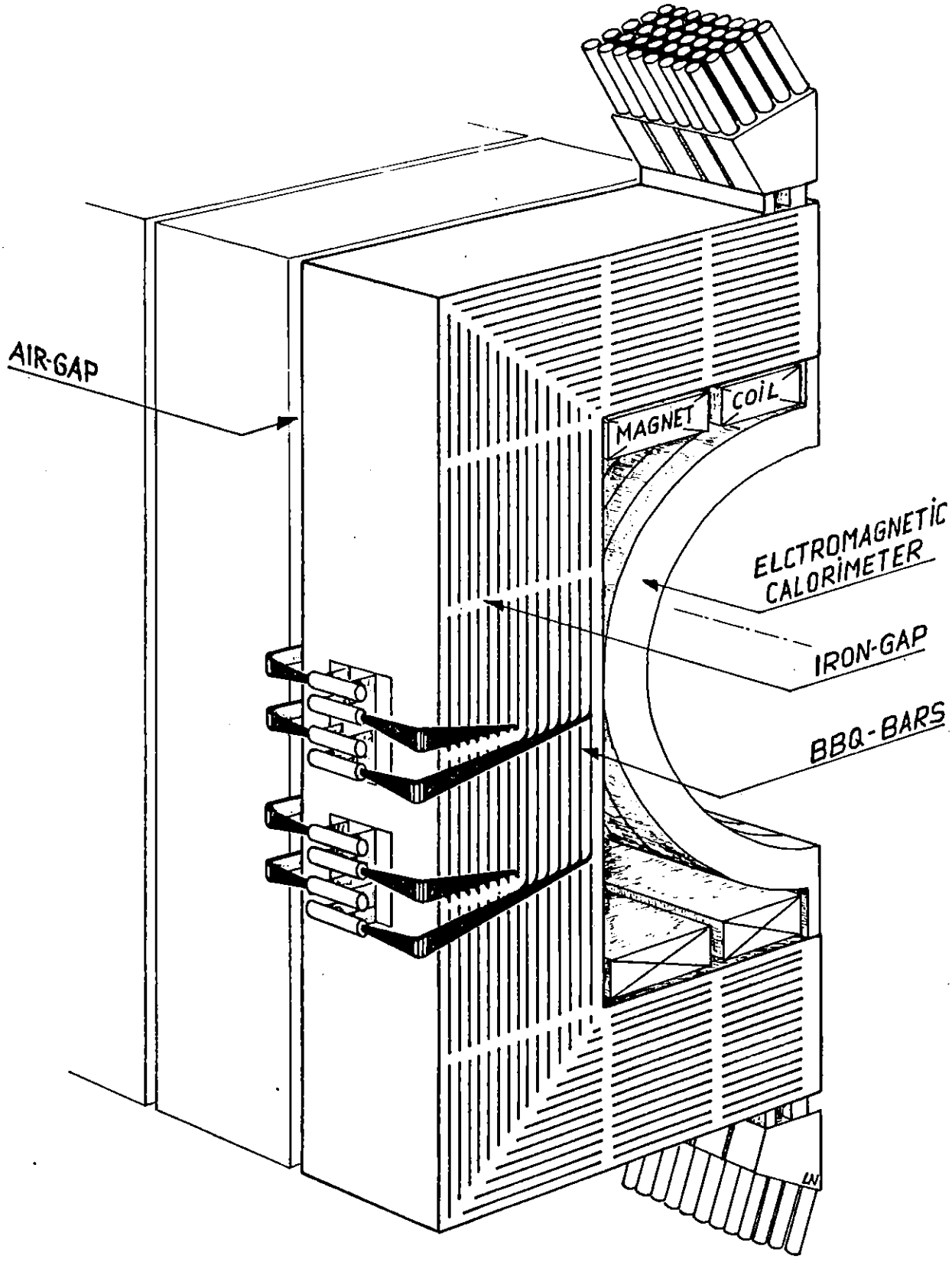
AIR-GAP
MAGNET
COIL
ELCTROMAGNETIC
CALORIMETER
IRON-GAP
BBQ-BARS

Fig. 8

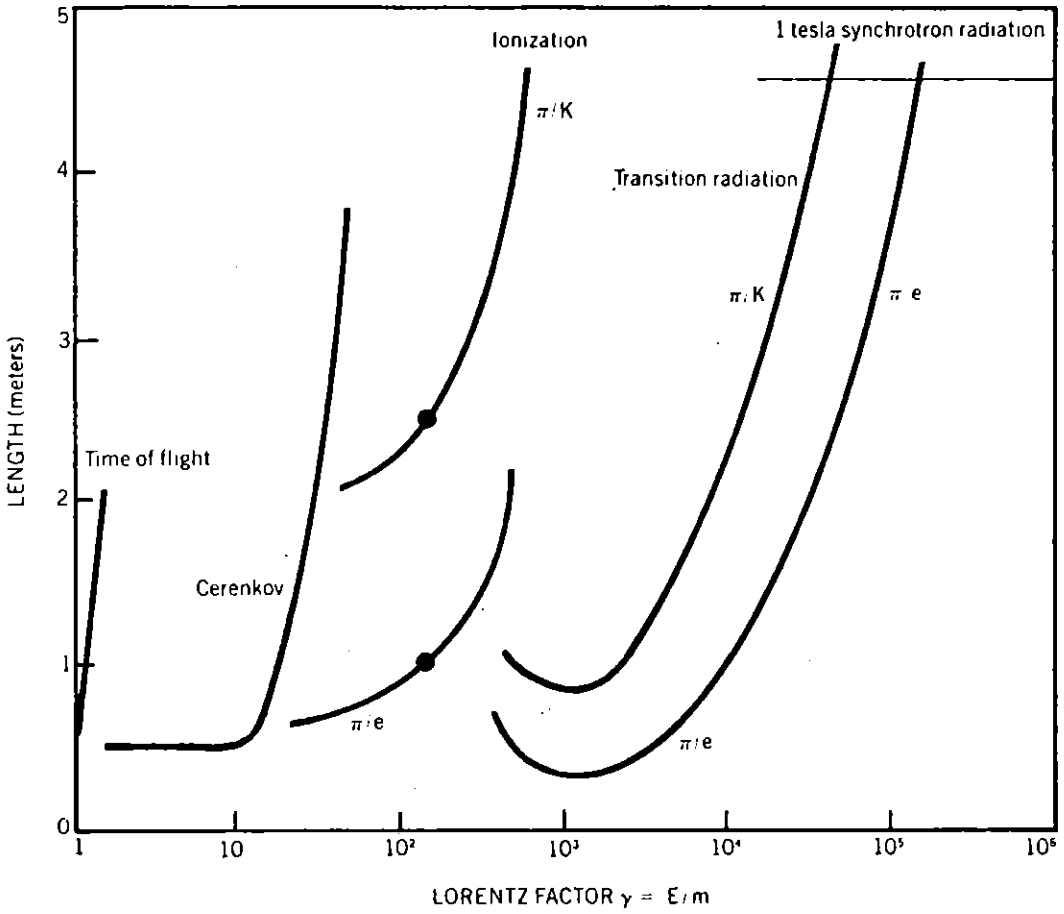
Ionization
1 tesla synchrotron radiation
π/K
Transition radiation
π/K
π e
Time of flight
Cerenkov
π/e
π/e
LENGTH (meters)
LORENTZ FACTOR γ = E/m
0
1
2
3
4
5
1
10
10²
10³
10⁴
10⁵
10⁶

Fig. 9

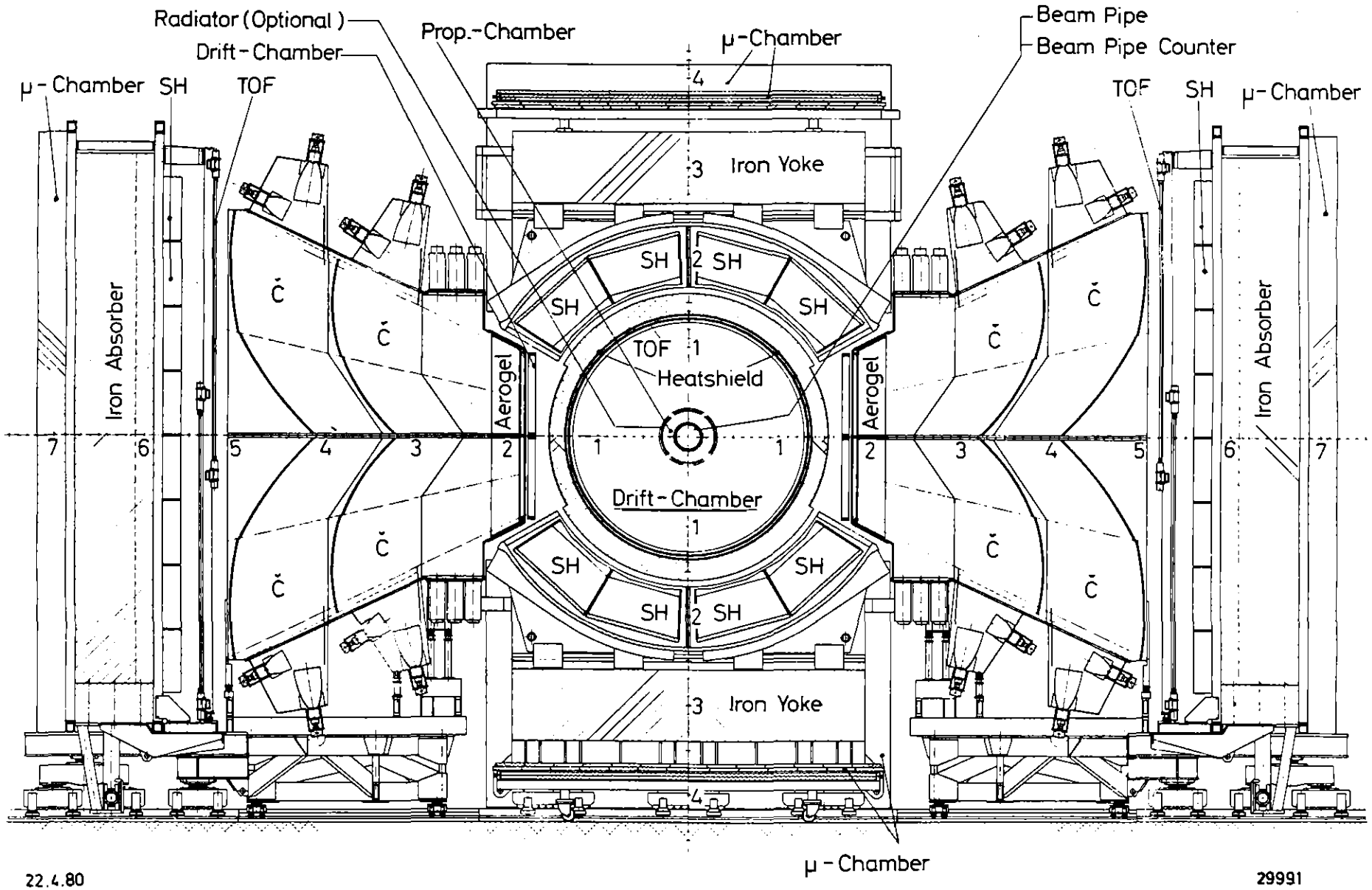
Radiator (Optional)
Drift-Chamber
Prop.-Chamber
μ-Chamber
Beam Pipe
Beam Pipe Counter
μ-Chamber
SH
TOF
TOF
SH
μ-Chamber
Iron Yoke
Iron Absorber
Č
SH
TOF
Heatshield
Aerogel
Aerogel
Drift-Chamber
Iron Yoke
Iron Absorber
μ-Chamber
22.4.80
29991

Fig. 10

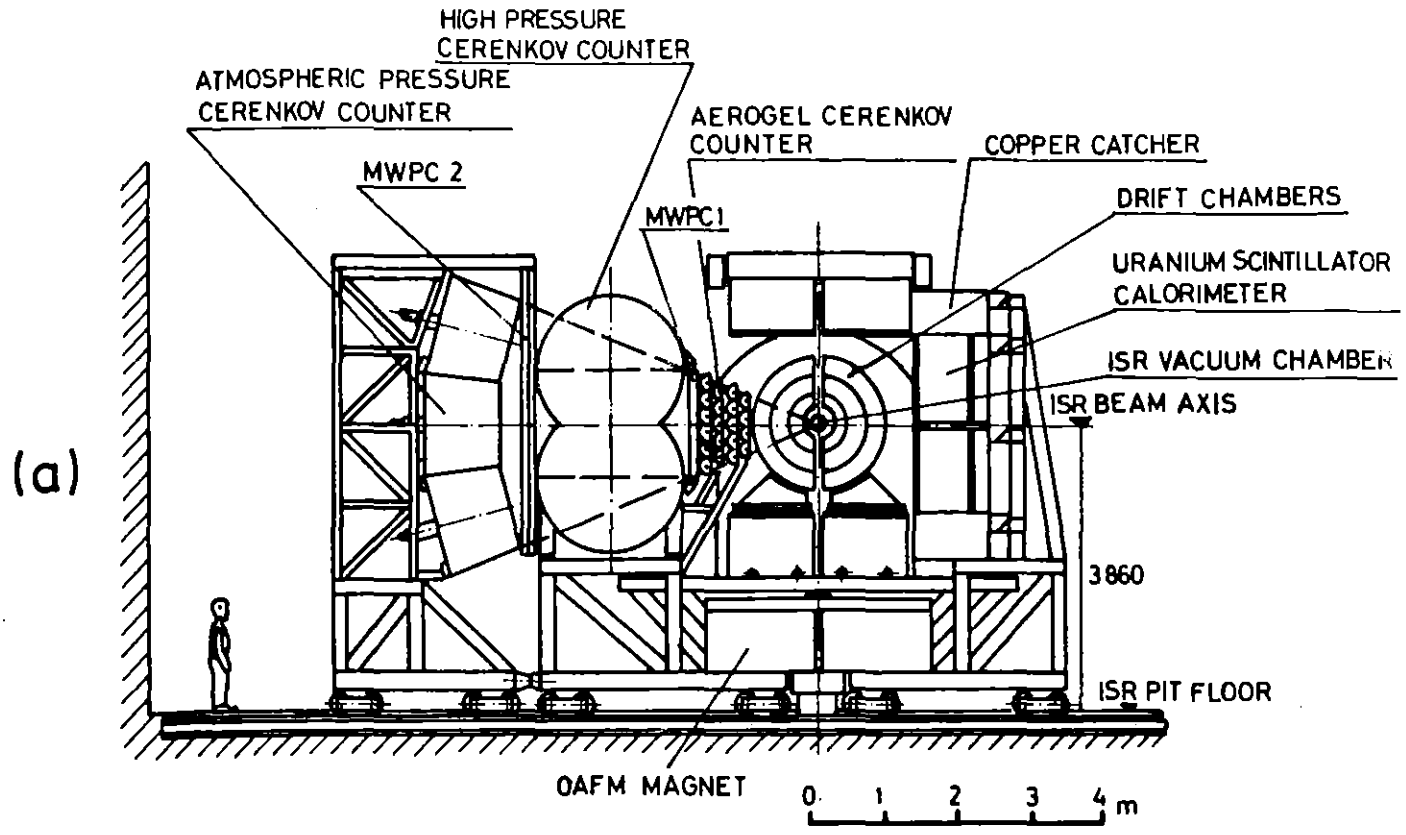
(a)
HIGH PRESSURE
CERENKOV COUNTER
ATMOSPHERIC PRESSURE
CERENKOV COUNTER
AEROGEL CERENKOV
COUNTER
COPPER CATCHER
MWPC 2
MWPC1
DRIFT CHAMBERS
URANIUM SCINTILLATOR
CALORIMETER
ISR VACUUM CHAMBER
ISR BEAM AXIS
3860
ISR PIT FLOOR
OAFM MAGNET
0 1 2 3 4 m

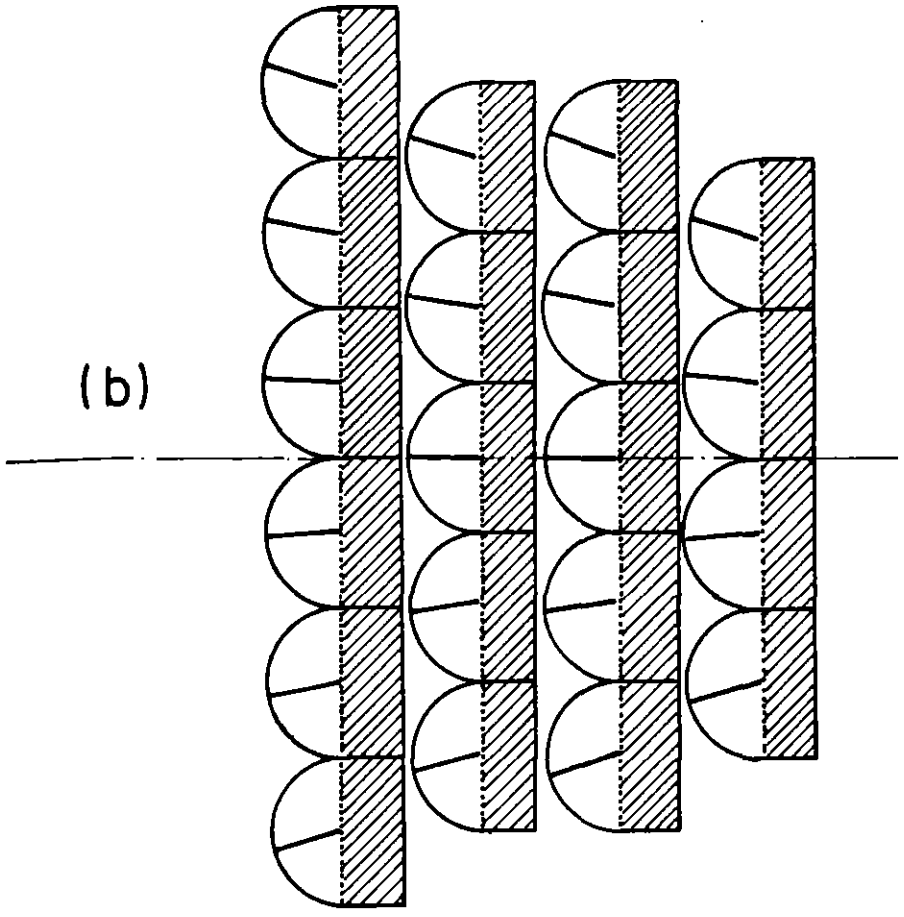
(b)

Fig. 11

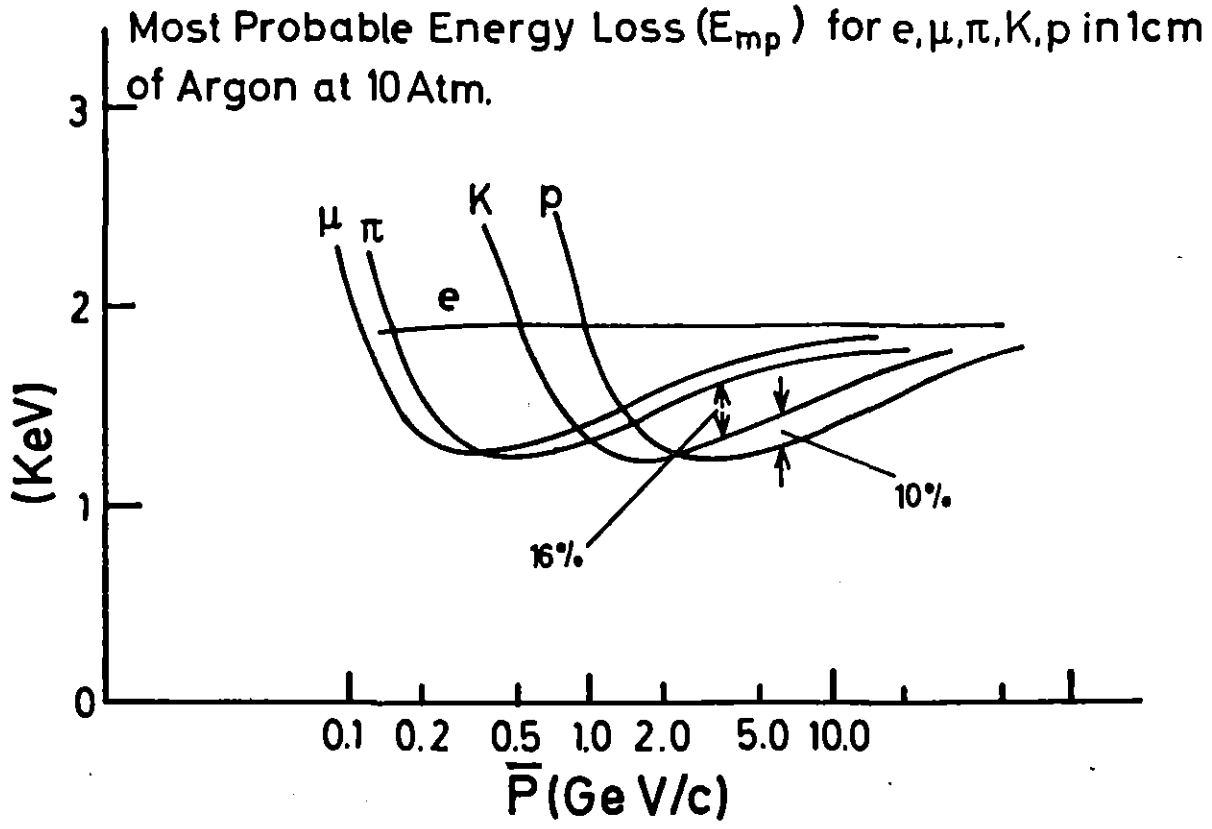
Most Probable Energy Loss (E_{mp}) for e, μ, π, K, p in 1cm of Argon at 10 Atm.
3
2
1
0
(KeV)
μ
π
K
p
e
10%
16%
0.1
0.2
0.5
1.0
2.0
5.0
10.0
$\bar{P}$ (Ge V/c)

Fig. 12

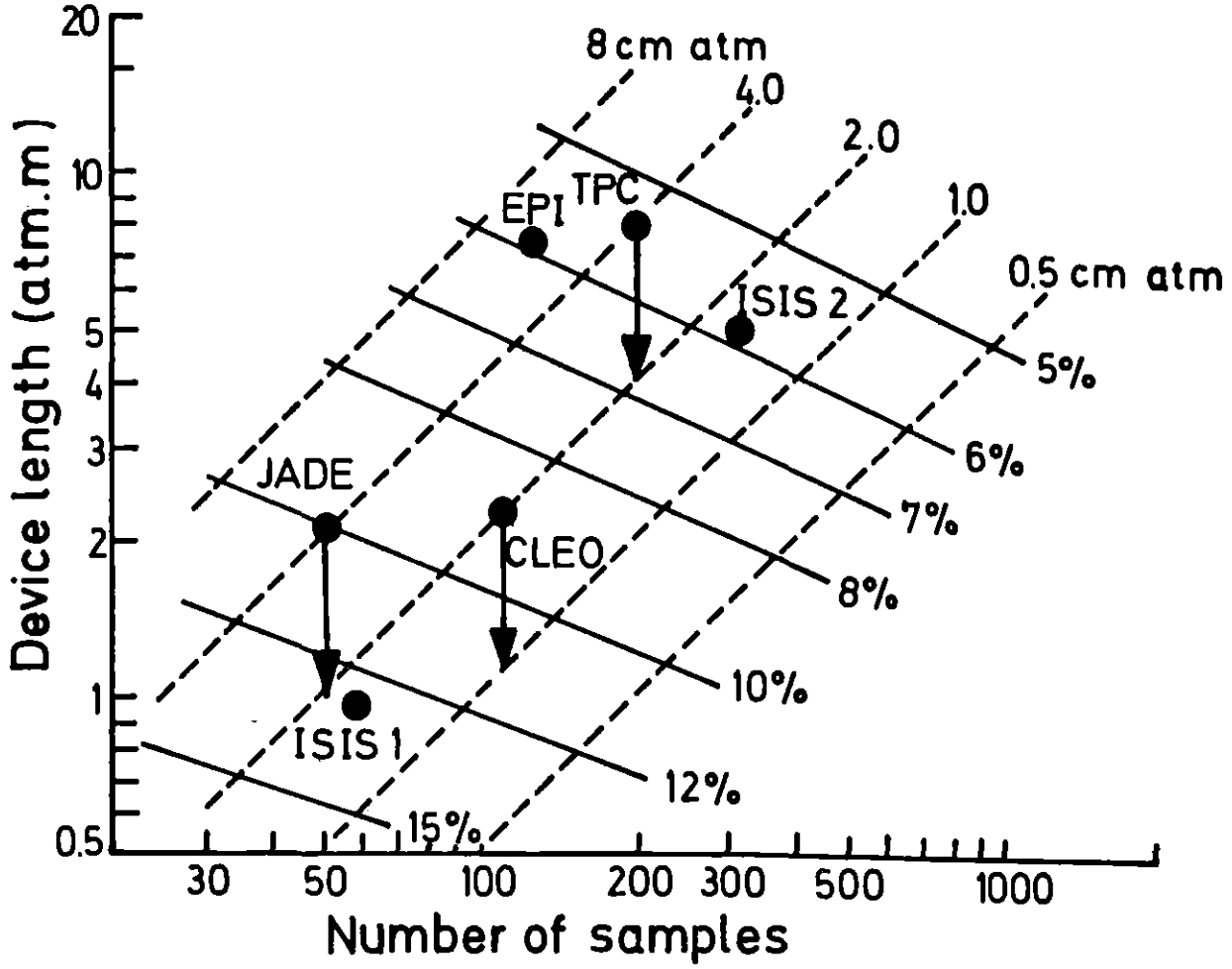
Device length (atm.m)
20
10
5
4
3
2
1
0.5
8 cm atm
4.0
2.0
1.0
0.5 cm atm
EPI
TPC
ISIS 2
JADE
CLEO
ISIS 1
5%
6%
7%
8%
10%
12%
15%
30
50
100
200
300
500
1000
Number of samples

Fig. 13